Neutron Spin Echo Spectroscopy at the NIST Center for Neutron Research

N. Rosov[1], S. Rathgeber[2,1], and M. Monkenbusch[3]

[1]**NIST Center for Neutron Research, Gaithersburg, MD 20899**
[2]**University of Maryland, College Park, MD 20742**
[3]**Forschungszentrum Jülich, Germany D-52425**

A Neutron Spin Echo (NSE) spectrometer is nearing completion at the NIST Center for Neutron Research. NSE spectroscopy measures the pair correlation function with respect to wave-vector transfer and time, unlike other neutron spectrometers, which measure the scattering as a function of wave-vector and energy transfer. The NIST NSE spectrometer can measure wave vector transfers from $0.01\,\text{Å}^{-1}$ to $2\,\text{Å}^{-1}$. The accessible time range for a particular setting of the spectrometer extends to nearly 10^{-7} s at the longest accessible wavelengths. We discuss here the expected properties of the NIST NSE spectrometer, provide a description of the strengths of NSE spectroscopy, and give some detail of the considerations necessary for designing a successful NSE experiment.

Introduction

Three high-resolution inelastic instruments are nearing completion at the NIST Center for Neutron Research (NCNR) [1]: a disk chopper time-of-flight spectrometer [2], a backscattering spectrometer [3], and a neutron spin echo (NSE) spectrometer. All three instruments will be available to researchers through reviewed proposals [4]. Both the NSE and Backscattering spectrometers will be operational in early 1999 and the Disk Chopper Spectrometer shortly thereafter.

The Disk Chopper and Backscattering spectrometers, like most other inelastic neutron spectrometers, measure the scattering function $S(Q,\omega)$, where Q is the wave-vector transfer and ω is the energy transfer of the scattering. The scattering function is the Fourier transform (in both time and length) of the real space pair correlation function. On the other hand, the NSE spectrometer measures the intermediate scattering function $I(Q,t)$ (the cosine transform of $S(Q,\omega)$). This is the same quantity that is measured by dynamic light scattering, albeit over a different time and Q range.

This paper provides a brief introduction to NSE, tailored to the particular details of the NIST NSE spectrometer, which has been optimized for the study of soft condensed matter systems. We will discuss how am NSE experiment is performed and outline the considerations required for choosing experimental systems.

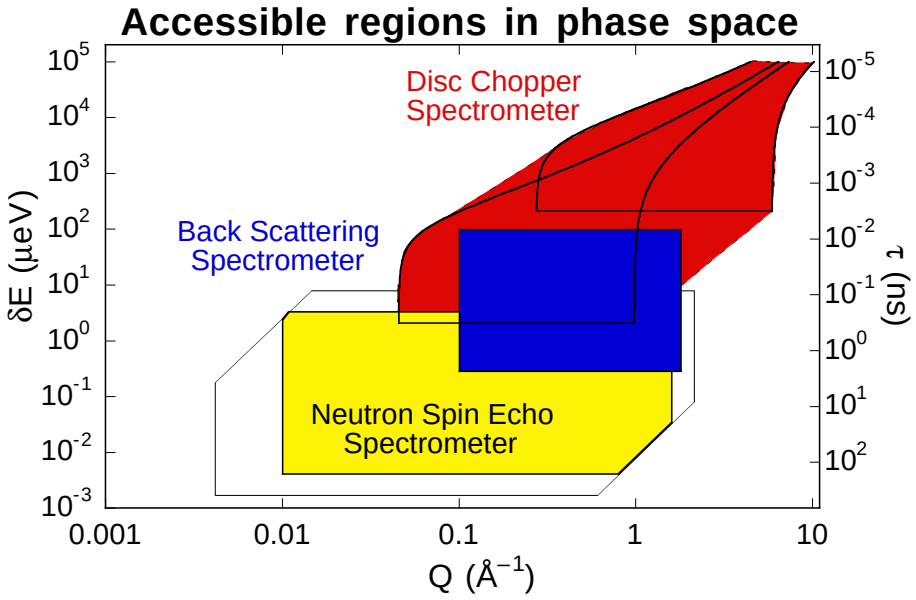

Figure 1: Phase space diagram indicating the region of accessibility for each of the three new inelastic instruments at the NIST Center for Neutron Research. The unshaded region around the NSE region indicates the effect of several planned improvements to the NSE instrument.

Experimental Realization of the Spectrometer

The design of the NCNR NSE spectrometer is based on that of the NSE spectrometer at the Forschungszentrum Jülich [5]. Exxon and the Forschungszentrum Jülich are additional members of the participating research team for constructing the spectrometer.

The NCNR reactor is a 20 MW heavy water reactor with a split core. A guide network is fed from a liquid H_2 cold source with an effective Maxwellian temperature of 45 K. The spectrometer is located at the end of guide NG-5, which is coated with ^{58}Ni. An optical filter [6] moves the end of the guide out of the direct line-of-sight of the reactor core, removing fast neutrons and core gammas from the beam, while allowing the transmission of neutrons with $\lambda > 4$ Å. A velocity selector roughly monochromates the neutron beam with

Table I: NCNR NSE operating characteristics at a glance

➤ **Velocity Selector**

- $\langle\lambda\rangle > 4.5$Å
- $8\% < \Delta\lambda/\lambda < 20\%$ (FWHM)

➤ **Polarizer**

- $3\theta_c$ Fe/Si supermirror "V" in guide.
- Maximum polarization for $\lambda > 5$ Å

➤ **Main Coils**

- $I_{max} = 440$ A
- $\mathcal{J}_{max} = 0.5\,\mathrm{T}\cdot\mathrm{m}$
- $0.1\,\mathrm{ns} < t < 30\,\mathrm{ns}$ (at 8 Å; $t_{min},\ t_{max} \propto \lambda^3$)

➤ **Sample region**

- Active area $5 \times 5\,\mathrm{cm}^2$
- Neutron flux $> 10^6\,\mathrm{n/cm^2/s}$ at 8 Å and $\Delta\lambda/\lambda = 10\%$
- Useful flux between 4.5 Å and 12 Å

➤ **Detector**

- $25 \times 25\,\mathrm{cm}^2$ area detector
- $Q_{min} \simeq 0.02\,\mathrm{Å}^{-1}$ at 8 Å
- Maximum scattering angle 100° ($Q_{max} \simeq 2.1\,\mathrm{Å}^{-1}$ at 4.5 Å)

$8\% < \Delta\lambda/\lambda < 20\%$ (FWHM) for mean wavelengths $\lambda > 4$ Å. The beam is polarized in the longitudinal direction by a Mezei cavity [7], with maximum polarization for $\lambda > 5$ Å.

We have performed preliminary measurements of the neutron flux at the end of the guide with a gold-foil technique. Measurements were made with the velocity selector set at three wavelengths, $\lambda = 6$, 9, and 12 Å with $\Delta\lambda/\lambda = 10\%$ FWHM; the results are shown in Figure 2, where the agreement between the measured results and the calculations is good at 9 Å; however, the difference between the results and calculations is around 30% at 6 Å and 12 Å. This difference may be attributed to neglect of wavelength-dependent absorption effects in the windows of the guides and the cold source.

The entire instrument is of amagnetic construction, and the computer program that operates the spectrometer contains an accurate description of the

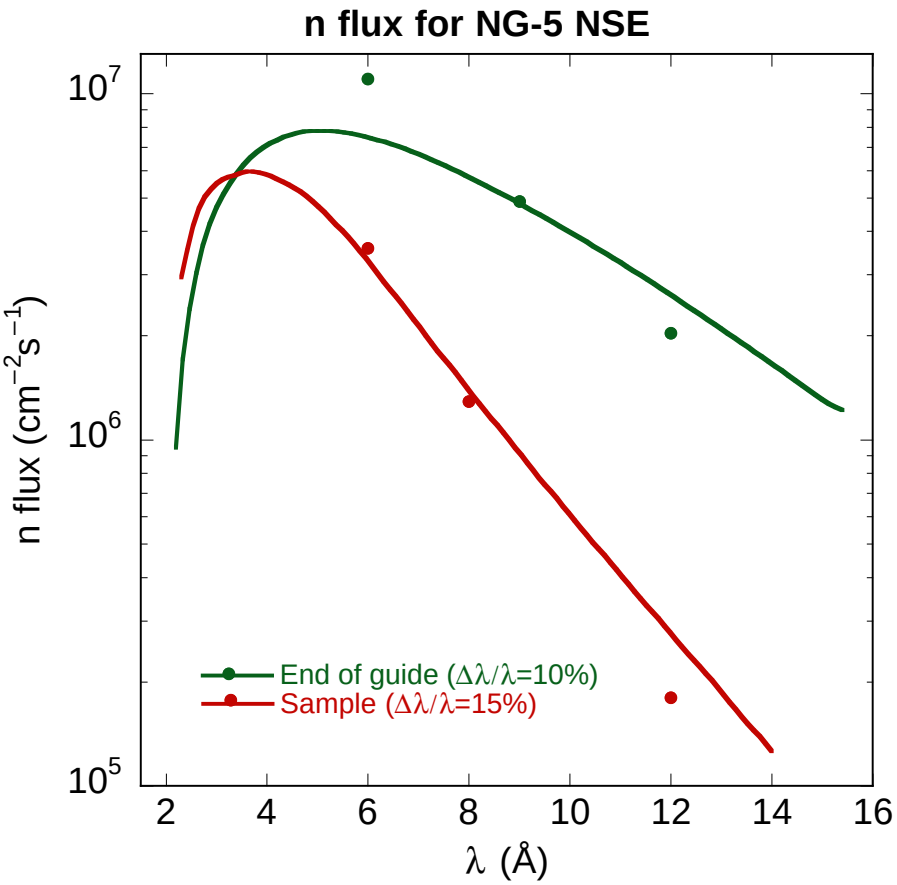

Figure 2: Calculated neutron fluxes (solid lines) at various points along neutron guide NG-5 to the NSE spectrometer with a $\Delta\lambda/\lambda = 10\%$ (FWHM) wavelength distribution: Just before taper; just after taper; at end of guide; and at sample position. The three large circles indicate the results of gold-foil measurements at the end of the guide.

current distributions, thereby allowing the total field distribution of the more than twenty coils to be calculated with sufficient accuracy to considerably reduce the time spent tuning the spectrometer. The main coils that provide a precession field contain compensation loops to rapidly reduce the on-axis field outside the solenoid. The inhomogeneities in the field are greatly reduced as a result, which decreases polarization losses, and so there is almost no decrease in the maximum accessible time at higher scattering angles.

The active sample area is $5 \times 5\,\mathrm{cm}^2$ (typical sample sizes for polymer studies are on the order of $3 \times 3 \times 0.3\,\mathrm{cm}^3$). This value is constrained by the flipper win-

dows and the sample environment. These can be extended somewhat; however, the sample size is ultimately constrained to 10 cm diameter by the active area of Fresnel-like correction elements inserted in the main coils. These correction elements allow off-axis and divergent neutrons to satisfy the echo condition (see Eq. 7) and thus allow the use of an area detector. This effectively increases the signal strength by a factor of twenty. The form of the sample is not constrained in principle by the NSE technique; however, the sample environment must not produce stray magnetic fields—e.g., from heating currents or construction materials—that might disrupt the measurement of the echo.

Principles of Neutron Spin Echo

The manipulation of the neutron spins through the spectrometer [8] is shown in Figure 3. After the beam is polarized, the neutron spins are rotated 90° by a $\pi/2$ flipper, which begins the precession of the neutron in the main solenoidal field.

In a perpendicular magnetic field B_1, a neutron spin will undergo precessions at a frequency $\omega_L = -\gamma_L B_1$, where $\gamma_L/(2\pi) = 29.16\,\mathrm{MHz/T}$. If a neutron is polarized perpendicularly to the axis of a solenoidal field, it will precess through an angle

$$\phi_i = \gamma_L \frac{m\lambda}{h} \int_i B_i(\ell) d\ell = \gamma_L \frac{m\lambda}{h} \mathcal{J}_i \tag{1}$$

where $\mathcal{J}_i$ is the field integral along solenoid i and λ is the wavelength of the neutron ($h/(m\lambda)$ is the neutron velocity v). Note that ϕ can only be determined to $\mathrm{mod}\,(2\pi)$.

For a beam of neutrons with an incident wavelength distribution $f(\lambda)$ and $\langle\lambda\rangle = \langle\lambda_1\rangle$, each neutron undergoes a spin precession of $\phi_1(\lambda)$ in the first arm of the spectrometer. The neutron beam, with its broad band of wavelengths, will completely depolarize in this first precession field.

After scattering from the sample, a neutron passes through a π-flipper, thereby changing its phase angle from $\phi \bmod (2\pi)$ to $-(\phi \bmod (2\pi))$ (see Figure 3b). Then, on passing through the second precession field, if the scattering is elastic and the two field integrals are the same, the beam recovers its full polarization at the second $\pi/2$ flipper, which rotates the spins back to the longitudinal direction, thereby stopping the precessions. The beam polarization is then analyzed and those neutrons with the correct spin state impinge on an area detector.

If the neutrons are scattered quasi-elastically from the sample (as is almost always the case for soft condensed matter research), changing wavelength by $\delta\lambda$, they will undergo a spin precession with phase angle ϕ_2 in the second arm of the spectrometer. The phase difference between the two arms of the spectrometer

$$\varphi = \phi_1(\lambda) - \phi_2(\lambda + \delta\lambda) \tag{2}$$

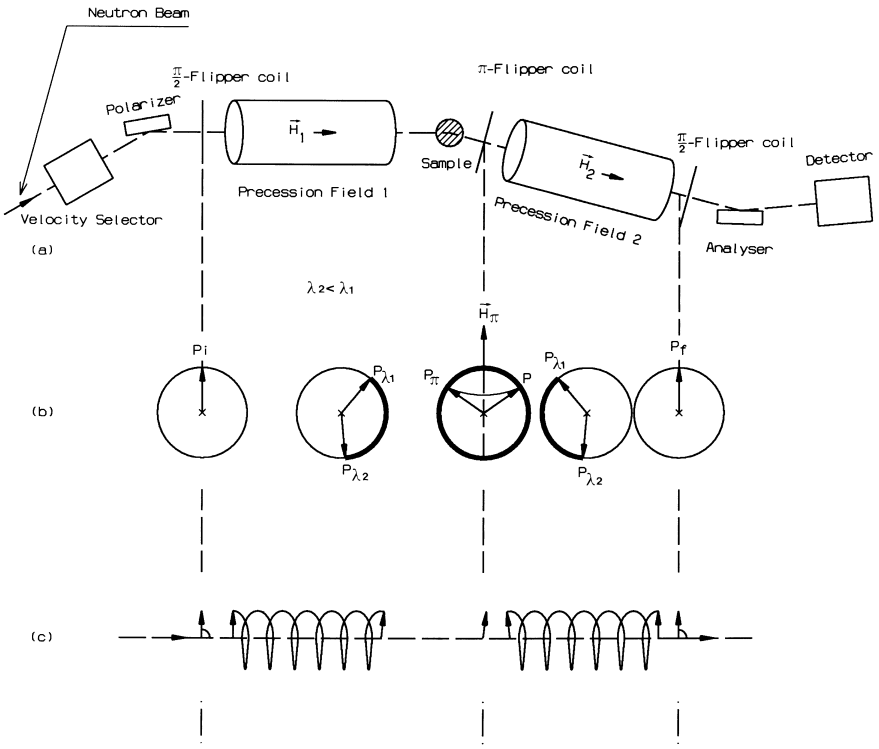

Figure 3: (a) Schematic of a Neutron Spin Echo spectrometer. The various components are discussed in the text. (b) Motion of the neutron spins in the precession region, looking downstream along the beam direction. (c) Motion of the neutron spins looking perpendicular to the beam direction. (Reproduced with permission from Reference [9].)

can be separated into two terms, one due solely to the inelasticity, the other due solely to the difference in the field integral of the two arms of the spectrometer,

$$\begin{aligned} \varphi &= \phi_1(\lambda) - \phi_1(\lambda+\delta\lambda) + \phi_1(\lambda+\delta\lambda) - \phi_2(\lambda+\delta\lambda) \\ &= \phi_1(\lambda) - \phi_1(\lambda+\delta\lambda) + \Delta\phi(\lambda+\delta\lambda). \end{aligned} \tag{3}$$

where

$$\Delta\phi(\lambda) = \phi_1(\lambda) - \phi_2(\lambda). \tag{4}$$

To first order in $\delta\lambda$ and $\Delta\phi$, the phase shift is composed of a term from the inelasticity and a term from the difference in the field integrals (recall from Eq. 1 that $\phi \propto \lambda$):

$$\begin{aligned}\varphi &= \phi_1(\langle\lambda_1\rangle)\frac{\lambda}{\langle\lambda_1\rangle} - \phi_1(\langle\lambda_1\rangle)\frac{\lambda+\delta\lambda}{\langle\lambda_1\rangle} + \Delta\phi(\langle\lambda_1\rangle)\frac{\lambda}{\langle\lambda_1\rangle} \\ &= \left(\phi_1(\langle\lambda_1\rangle)\delta\lambda + \Delta\phi(\langle\lambda_1\rangle)\lambda\right)/\langle\lambda_1\rangle. \end{aligned} \tag{5}$$

The average over the beam, in our quasi-elastic approximation, gives $\langle\delta\lambda\rangle = 0$, and so

$$\langle\varphi\rangle = \Delta\phi(\langle\lambda_1\rangle). \tag{6}$$

The spectrometer is therefore in the echo condition when there is no difference between the spin precession angles of the two arms of the spectrometer, *i.e.*, $\langle\varphi\rangle = 0$, which only holds when

$$\mathcal{J}_1 = \mathcal{J}_2. \tag{7}$$

The inelasticity of the scattering can be written as a change in wavelength

$$\hbar\omega = E_1 - E_2 = \frac{h^2}{2m}\left(\frac{1}{\lambda^2} - \frac{1}{(\lambda+\delta\lambda)^2}\right), \tag{8}$$

where, to first order in $\delta\lambda$,

$$\hbar\omega = \frac{h^2}{m}\frac{\delta\lambda}{\lambda^3}. \tag{9}$$

Due to the quantum nature of the neutron spin, only one component of the spin, call it z, can be determined. The polarization of the scattered beam is

$$\begin{aligned}\langle P_z\rangle &= \langle\cos(\varphi)\rangle \\ &= \int f(\lambda)d\lambda \times \\ &\qquad \int S(Q,\omega)\cos\left[\left(\phi_1(\langle\lambda_1\rangle)\frac{m\lambda^3}{2\pi h}\omega + \Delta\phi(\langle\lambda_1\rangle)\lambda\right)/\langle\lambda_1\rangle\right]d\omega. \end{aligned} \tag{10}$$

Since we have assumed $S(Q,\omega)$ is a quasi-elastic scattering law, which is essentially an even function of ω, the polarization of the beam is

$$\begin{aligned}\langle P_z\rangle &= \int f(\lambda)\cos(\Delta\phi(\langle\lambda_1\rangle)\lambda/\langle\lambda_1\rangle)d\lambda \times \\ &\qquad \int S(Q,\omega)\cos\left(\phi_1(\langle\lambda_1\rangle)\frac{m\lambda^3}{2\pi h\langle\lambda_1\rangle}\omega\right)d\omega \\ &= \int f(\lambda)\cos(\Delta\phi(\langle\lambda_1\rangle)\lambda/\langle\lambda_1\rangle)d\lambda \times \int S(Q,\omega)\cos(\omega t)d\omega \end{aligned} \tag{11}$$

where

$$t = \phi_1(\langle\lambda_1\rangle)\frac{m\lambda^3}{2\pi h\langle\lambda_1\rangle} = \gamma_L\left(\frac{m}{h}\right)^2\frac{\lambda^3}{2\pi}\mathcal{J}_1 \tag{12}$$

is the Fourier time.

By adjusting the field so that the echo condition (Eq. 7) is met, the beam polarization is

$$\langle P_z \rangle = \int f(\lambda) d\lambda \times \int S(Q,\omega)\cos(\omega t) d\omega = \int f(\lambda) I(Q,t) d\lambda. \tag{13}$$

In many experimental cases $I(Q,t)$ varies very slowly with λ and so can be removed from the integrand; in these cases, Neutron Spin Echo spectroscopy directly measures the intermediate scattering function, the energy cosine transform of the scattering function. In these situations, it is not even necessary to determine the wavelength distribution; however, if the wavelength distribution is strongly affected by the scattering process, for example by absorption, then the wavelength distribution must be determined.

Even if the condition of small energy transfers does not hold, a linear relationship between the phase angle shift φ and the energy transfer $\delta\omega$ can be derived for the non-quasi-elastic case, *viz.*

$$\varphi - \overline{\varphi} = t \times (\omega - \overline{\omega}). \tag{14}$$

Here $\overline{\omega} = \overline{\omega}(\langle\lambda_1\rangle, \langle\lambda_2\rangle)$ is the average energy transfer and $\overline{\varphi} = \overline{\varphi}(\langle\lambda_1\rangle, \langle\lambda_2\rangle)$ the average phase angle shift associated with the average wavelengths $\langle\lambda_i\rangle$ $(i = 1, 2)$ before and after the scattering process. The assumption necessary for derivating Eq. 14 is that the wavelength distribution of the neutrons contributing to the echo must be limited:

$$\Delta\lambda_i = \lambda_i - \langle\lambda_i\rangle \ll \langle\lambda_i\rangle \text{ for } i = 1, 2. \tag{15}$$

The echo condition becomes

$$\langle\lambda_1\rangle^3 \mathcal{J}_1 = \langle\lambda_2\rangle^3 \mathcal{J}_2 \tag{16}$$

and in Eq. 5, φ must be replaced by $(\varphi - \overline{\varphi})$ as given in Eq. 14.

To fulfill Eq. 15, the transmission function of the NSE spectrometer has to be limited to a certain wavelength range. This is mainly done by the velocity selector in the incoming beam and by the limited wavelength acceptance of the analyzer for processes causing a broadening of the wavelength distribution in the scattered beam. For more detailed information see the article by Mezei in Ref. [8].

We will see below, however, that the most powerful application of NSE lies in the field of quasi-elastic scattering with $\overline{\omega} = 0$, where the first derivation suitably describes the function of the NSE spectrometer.

Applications

There are two simple ways to perform NSE scans: In one, not so frequently used, the time parameter (that is, the field integral) is set as small as possible

(although the field must be larger than any stray fields that might depolarize the beam) and so the second term in Eq. 11 reduces to $S(Q)$,

$$\langle P_z \rangle = \int S(Q) f(\lambda) \cos(\Delta\phi(\langle\lambda_1\rangle)\lambda/\langle\lambda_1\rangle) d\lambda \tag{17}$$

By varying the difference in the field integrals, one can measure the cosine transform of $S(Q)f(\lambda)$, which, given a constant or slowly varying $S(Q)$, is a cosine function, with a period proportional to $\langle\lambda_1\rangle^{-1}$, modulated by the cosine transform of the wavelength distribution. This scan is often used to "prove" that an NSE instrument is working (see Figure 4) and, more important, to correct either for the effect of strong absorption (or multiple scattering) from the sample or for a strong Q-dependence in the scattering.

The other scan, commonly used for measurements in polymer or similar systems, is taken by setting the spectrometer to the echo condition, which gives Eq. 13, and so the intermediate scattering function. In practice (see Figure 4), the counting rate is measured for several phase current values near the echo position, then fitted to the modulated cosine of Eq. 17 to give the echo amplitude A. The effect of the less-than-perfect efficiency of the flippers, the polarizer, and the analyzer is removed by measuring the count rates with the $\pi/2$-flippers off and the π-flipper both off and on, giving $N_{\rm up}$ and $N_{\rm down}$, respectively. The measured value of the polarization of the scattered beam at the echo point $\langle P_z \rangle_M$ is then determined by

$$\langle P_z \rangle_M = \frac{2A}{N_{\rm up} - N_{\rm down}}. \tag{18}$$

Inhomogeneities in the magnetic field may further reduce the polarization. As these inhomogeneities are not correlated with $S(Q,\omega)$ or $f(\lambda)$, their effect may be simply divided out by measuring the polarization from a purely elastic scatterer $\langle P_z \rangle_M^E$. The value of $I(Q,t)$ is then given by

$$\frac{I(Q,t)}{I(Q,0)} = \langle P_z \rangle = \frac{\langle P_z \rangle_M}{\langle P_z \rangle_M^E}. \tag{19}$$

The time is varied, according to Eq. 12, by changing the field in the main coils.

This procedure is particularly useful for measuring quasi-elastic processes or processes at small energies where discriminating the scattering of interest from any elastic scattering is important. On a conventional spectrometer, deconvolving the instrumental energy lineshape from the physical lineshape can be quite difficult. However, a convolution in ω-space becomes a simple product in the time domain. Rather than performing highly elaborate lineshape analyses in the energy domain to determine, for instance, if a process is elastic or quasi-elastic, one can merely note if the NSE signal is constant or decays with time. Figure 5 shows several scenarios where the inelastic scattering might be determined in the time domain by NSE.

Typical spectra observed by incoherent neutron scattering for a vibrational process show in the energy domain as two inelastic lines with width Γ centered at

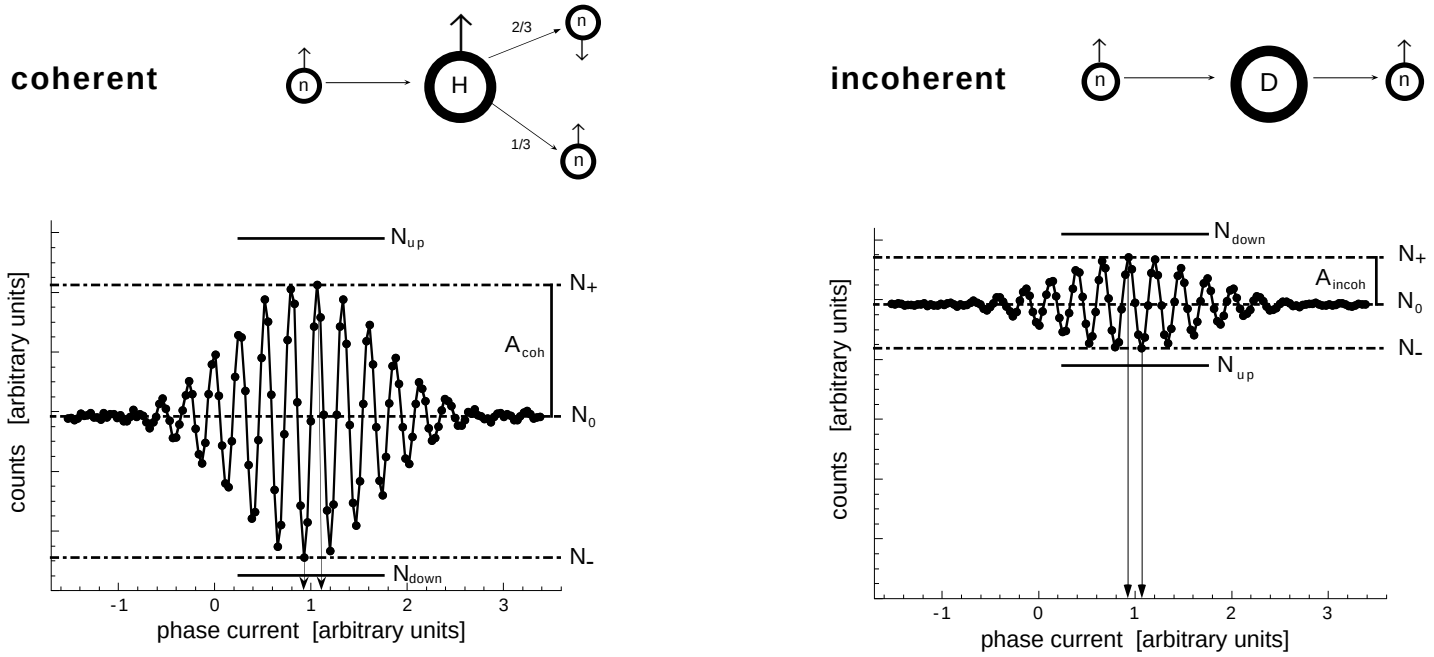

Figure 4: NSE signal as a function of the phase difference between the incident and scattered beams. The upper part of the figure shows the principle difference, in the case of deuterons and protons, between the scattering from a nucleus with and without nuclear spin. The lower part shows the NSE signals obtained in both cases—the count rate is plotted against the current of the phase correction coil. $A_{\rm coh}$ *and* $A_{\rm incoh}$ *are the echo amplitudes for coherent and incoherent scattering,* N_0 *is the average count rate outside the echo,* N_+ *and* N_- *are the maximal and minimal count rates with the* $\pi/2$*-flippers on, and* $N_{\rm up}$ *and* $N_{\rm down}$ *are the count rates of spin-up (*π*-flipper off) and spin-down (*π*-flipper on) measurements made with the* $\pi/2$*-flippers off.*

ω_0 and $-\omega_0$, as well as an elastic feature that comes from the center of mass. A Fourier transformation into the time domain yields a damped cosine oscillating around a nonzero average value. Rotational motions, which show broader quasi-elastic features around the elastic line of the center of mass in the ω-domain, are also observed by incoherent scattering. For a simple Lorentzian-line shape in time-space a single exponential decay to a nonzero plateau value for long-time limit would be observed.

It is possible in principle to measure the incoherent intermediate structure factor $I_{\rm incoh}(Q,t)$ with the classical NSE spectrometer design (such as that at NCNR); however, in practice it can be difficult to measure $I_{\rm incoh}(Q,t)$ in a reasonable measuring time. There are three sources of incoherent scattering:

- isotopic variation in the nuclear cross-section;
- uncorrelated motions, e.g., noninteracting rotators; and
- variation in the nuclear cross section due to the nuclear spin.

All of these reduce the signal intensity since all incoherent scattering is spread out isotropically in a solid angle of 4π.

The consequences of spin-incoherent scattering, which can have a significantly deleterious effect on the NSE signal, are shown in Figure 4. Spin-incoherent scattering causes, with a nucleus-dependent probability, a spin flip of both the inelastically and elastically scattered neutrons, *e.g.*, 2/3 of the neutrons scattered from H undergo a spin flip, whereas deuterium, which has no nuclear spin, has no influence on the neutron spin.

Note that this spin flip caused by spin-incoherent scattering is not the same as that occurring in the π flipper in the sample region. The π flipper changes the phase of the neutron from $\phi + 2n\pi$ to $-\phi + 2n\pi$, so that, for instance, on elastically scattering, with the first and second field integrals equal, the neutron ends up at the second $\pi/2$ flipper with phase $-\phi+2n\pi+\phi+2n\pi = 4n\pi$, that is, the original phase. In spin-incoherent scattering precesses, some fraction of the spins (2/3 in the case of H-scattering) are flipped by 180°, that is, from $\phi+2n\pi$ to $\phi + (2n+1)\pi$ and then to $-\phi + (2n+1)\pi$ by the π-flipper. These spins end up at the second $\pi/2$ flipper with phase $-\phi + (2n+1)\pi + \phi + 2n\pi = \pi + 4n\pi$, and produce an echo that is reversed with respect to the non-spin-incoherent case. The overall echo amplitude is a superposition of the signals with opposite sign from the spin-flipped and non-spin-flipped neutrons, and so is reduced. For scattering from protons, the final signal is $-1/3$ of the signal from the non-spin-incoherent scattering case; the background is strongly increased as well, reducing the signal-to-noise ratio considerably. If, in addition, there is some coherent scattering present, the spin-incoherent and coherent cross sections have opposite signs for the echo signal and so reduce the echo signal in a way that cannot be decomposed.

The main application of NSE spectroscopy is therefore to measure the intermediate coherent scattering function $I_{\rm coh}(Q,t)$, the coherent density fluctuations that correspond to some SANS intensity pattern. This type of scattering may

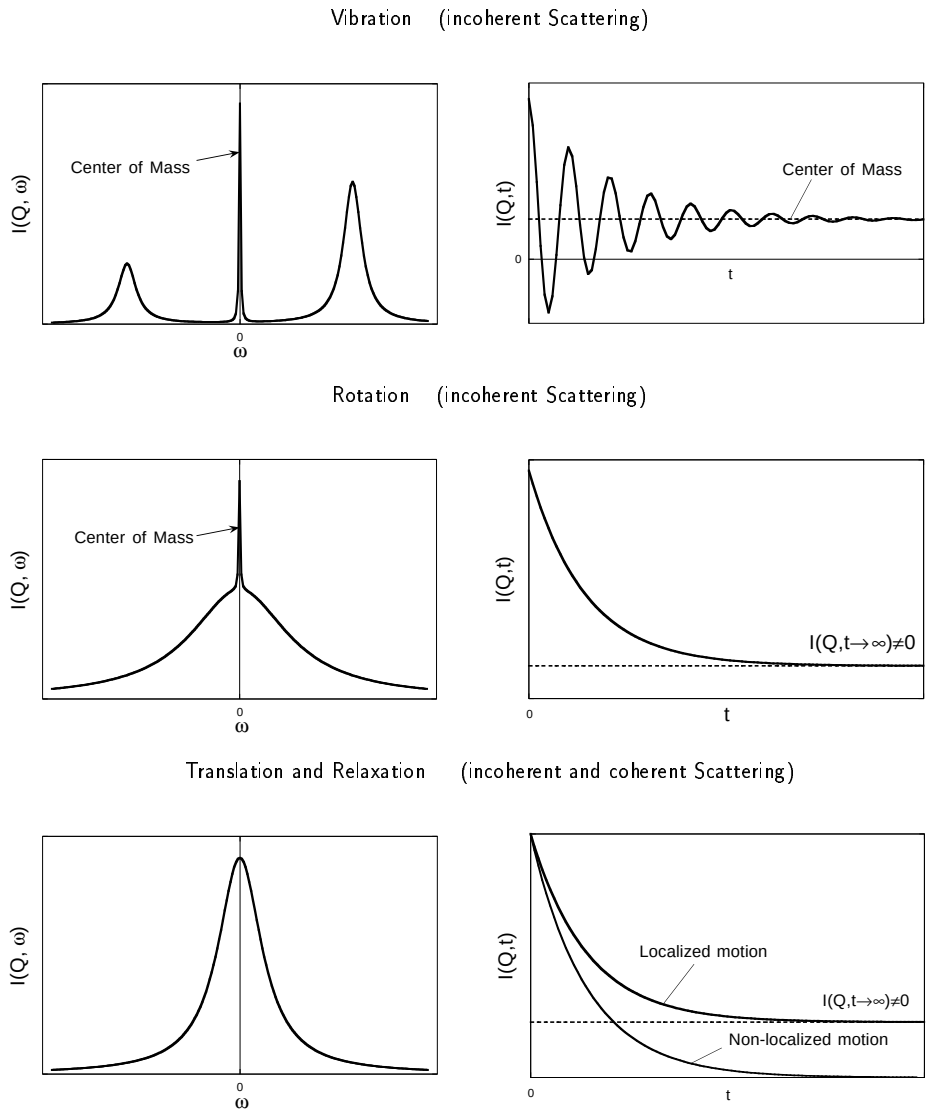

Figure 5: A comparison of typical scattering spectra obtained by inelastic neutron scattering in the energy and time domains for (a) vibrational, (b) rotational, (c) translational, and (d) relaxational motion.

be orders of magnitude more intense than the incoherent contributions. In general, however, measurements on polymeric and biological systems require that the some part of the sample be deuterated. The degree of deuteration is an practical issue that involves optimizing contrast against incoherent background and depends in part on the amount of beam time available for a particular experiment.

Translational and relaxational motions that can be observed in coherent scattering result in a broad quasi-elastic feature around $\omega = 0$, which gives, in the case of a Lorentzian lineshape, a simple exponential decay in the time domain. If the motion is localized in space, the final plateau value of the $I_{\mathrm{coh}}(Q,t)$ is nonzero.

We can summarize that the great advantage of NSE spectroscopy lies in investigations of *aperiodic relaxation dynamics*. On mesoscopic time scales well separated from atomic time scales, these processes show broad quasi-elastic features in frequency space, but a featureless decaying structure in the time domain.

Within these constraints, NSE spectroscopy covers a wide range of applications. In classical solid state physics, critical scattering in the fields of magnetism [10, 11] and structural phase transitions [12, 13] mainly have been investigated. But NSE spectroscopy has also shown to be an extremely useful tool for probing the dynamics of soft matter. In the case of polymer systems, the single chain relaxation of polymers of various structures (stars, cyclic, diblock-copolymers, linear polymers, micelles) were investigated [14, 15, 16]. NSE also plays an outstanding role in the investigation of the relaxation processes in glassy systems [17]. Beyond this, studies have been performed on complex fluids—shape and size fluctuations of microemulsions [18, 19] and on systems with biological importance [20].

References

[1] see *J. Res. Nat. Inst. Stand. Technology* **1993**, *98*.

[2] Altorfer, F. B.; Cook, J. C.; Copley, J. R. D. *Mat. Res. Soc. Symp. Proc.* **1995**, *376*, 119.

[3] Gehring, P. M.; Neumann, D. A. *Physica B* **1998**, *241–243*, 64–70.

[4] Information on submitting proposals may be obtained on the NCNR web site `<http://www.ncnr.nist.gov/>` or by contacting one of the authors: `nrosov@nist.gov` or `silke.rathgeber@nist.gov`.

[5] Monkenbusch, M.; Schätzler, R.; Richter, D. *Nucl. Instr. Meth. Phys. Res. A* **1997**, *399*, 301–323.

[6] Copley, J. R. D. *J. Neutron Res.* **1994**, *2*, 95.

[7] Krist, T.; Lartigue, C.; Mezei, F. *Physica B*, **1992**, *180*, 1005–1006.

[8] A much more complete description of NSE can be be found in *Neutron Spin Echo*; Editor, F. Mezei, Lecture Notes in Physics, vol. 128; Springer-Verlag: Berlin, 1980. The present outline follows that given in the article by J. B. Hayter, pp 53–65.

[9] Rathgeber, S. Ph. D. Thesis, University of Aachen, Nordrhein-Westfalen, Germany, 1997.

[10] Bewley, R. I.; Stewart, J. R.; Ritter, C.; Schleger, P.; Cywinski, R. Physica B **1997**, *234*, 762–763.

[11] Sarkissian, B. V. B. *Philos. Mag. B* **1996**, *74*, 211–217.

[12] Kakurai, K.; Sakaguchi, T.; Nishi, M.; Zeyen, C. M. E.; Kashida, S.; Yamada, Y. *Phys. Rev. B* **1996**, *53*, R5974–R5977.

[13] Durand, D.; Papoular, R.; Currat, R.; Lambert, M.; Legrand, J. F.; Mezei F. *Phys. Rev. B* **1991**, *43*, 10690–10696.

[14] Ewen, B.; Richter, D. *Adv. Polym. Sci.* **1997** *134*, 1–129.

[15] Richter, D.; Willner, L.; Zirkel, A.; Farago, B.; Fetters, L. J.; Huang, J. S. *Macromolecules* **1994**, *27*, 7437–7446.

[16] Farago, B.; Monkenbusch, M.; Richter, D.; Huang, J. S.; Fetters, L. J.; Gast, A. P. *Phys. Rev. Lett.* **1993**, *71*, 1015–1018.

[17] Arbe, A.; Richter, D.; Colmenero, J.; Farago, B. *Phys. Rev. E* **1996**, *54*, 3853–3869.

[18] Farago, B. *Physica B* **1996**, *226*, 51–55.

[19] Farago, B.; Richter, D.; Huang, J. S.; Safran, S. A.; Milner, S. T. *Phys. Rev. Lett.* **1990**, *65*, 3348–3351.

[20] Pfeiffer, W.; Konig, S.; Legrand, J. F.; Bayerl, T.; Richter, D.; Sackmann, E. *Europhys. Lett.* **1993**, *23*, 457–462.

Erratum

1. The scattering diagrams in Figure 4 have been reversed: The scattering from H should be with the incoherent subfigure and the scattering from D should be with the coherent subfigure.